5

Single charge transport in graphene

Running head: Single charge transport in graphene

> (i) The corrections made in this section will be reviewed and approved by master copier.

Dong Su Lee

Institute of Advanced Composite Materials, Korea Institute of Science and Technology (KIST), Bongdong-eup, Jeonbuk, South Korea

5.1 Introduction

Generally, in electronic devices, the discreteness of electrons cannot be seen in a macroscopic transport measurement. In other words, the behaviors of individual electrons are hidden in an averaged view so that one can measure only statistical observables. Ways to disclose the behaviors of individual charges in transport are related to quantum states in which the wavefunctions of particles are bound, for example induced by (i) Coulomb repulsion in a metallic island, that is, single electron transistors (SETs); (ii) quantum confinement due to the size effect, that is, quantum dots (QDs); and (iii) occupation of charges in incompressible condensates at high magnetic fields, that is, the quantum Hall effect (QHE). The investigation of the former two requires small devices in nanometer scale, but the last quantum Hall effect [1] can be observed in macroscopic devices even over hundreds of micrometers. Interestingly, as recent studies demonstrated, the physics behind the quantum Hall localization is in the same principle as that of SETs or QDs [2]. The single charge behaviors have been explored mainly in systems with massive particles, conventional metals, and semiconductors. After graphene has been brought into practical realization by mechanical exfoliation form crystalline graphite, this two-dimensional system with massless particles has aroused the interest of the studies on single *massless* charge transport behaviors.

As an overview, in Section 5.2, an introduction about single charge tunneling behavior will be given. In Section 5.3, Electrical properties of graphene will be discussed. A review of studies on single charge transport behaviors of massless particles in graphene will be given in Section 5.4. Quantum Hall localization behaviors in graphene will be discussed, in particular, with respect to Coulomb blockade physics governing the charge tunneling into the compressible QDs, in Section 5.5.

5.2 Single charge tunneling

5.2.1 Single charge tunneling and Coulomb blockade

When electrons' pathways in a conducting channel are blocked by an insulating gap with a capacitance of C, the conduction through the gap occurs by quantum tunneling if the tunneling resistance of the insulating barrier R_T is sufficiently larger than the resistance quantum of $h/e^2 \approx 25.813$ kΩ, where h is the Planck's constant and e is the electron's charge. A charging energy scale ($E_c \equiv e^2/C$) plays an important role in the conduction through the barrier in the regime where the thermal energy $k_B T$ is much smaller than E_c. Here, k_B is the Boltzmann constant and T the temperature. Therefore, single charge tunneling occurs at low temperatures. A common device used to study such single charge tunneling behavior is a single electron transistor (SET), which is composed of a metallic "island" and three electrodes of source, drain, and gate. See Fig. 5.1A. These are the same components as those in conventional transistors. The island is completely isolated from the outer environment except for the weak couplings with the three electrodes.

alt-text: Fig. 5.1
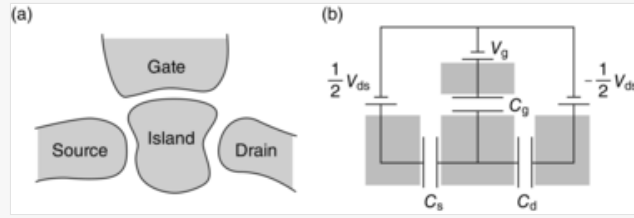
A schematic drawing of a single electron transistor (A) and its equivalent circuit (B).

In order to inject one additional electron into the island; for example, from N_e to $(N_e + 1)$, where N_e is the number of electrons occupied the states in the island; an additional energy is required due to the Coulomb repulsion, which amounts the difference of electrochemical potentials for $(N_e + 1)$ and for N_e electrons, $\Delta E_{add} = \mu_{N+1} - \mu_N$. Here, the electrochemical potential reads as [3, 4]

$$\mu_N = E_c \left(N_e - \frac{1}{2} \right) + e\alpha_g V_g \tag{5.1}$$

The gate influence factor is defined as $\alpha_g \equiv C_g/C_\Sigma$, where the total capacitance $C_\Sigma = C_s + C_d + C_g$ and C_s, C_d, and C_g are the capacitances of source, drain, and gate, respectively. When the size of the island is small enough, the discrete energy states emerge as the level spacing exceeds the thermal broadening. The island is then considered as an artificial atom or a quantum dot (QD), and the single-particle energy of the N electrons in the QD, E_N, cannot be ignored according to Pauli's exclusion principle. The energy required for charge injection into the QD equals the sum of interaction-induced energy (charging energy) and the single-particle energy spacing (frequently termed as quantum confinement); $\Delta_N = \varepsilon_{N+1} - \varepsilon_N$, where ε_N is the single-particle energy, $\Delta E_{add} = E_c + \Delta_N$. As the electrochemical potential of the island is tuned by modulation of the gate voltage V_g with a small source-drain bias V_{ds}, the discrete energy levels in the island gradually shift up or down. When the chemical potentials of the source and drain electrodes $(\mu_s \approx \mu_d)$ are placed in the region of the gap between the discrete levels of the island, electrons cannot tunnel from the drain to the island due to the strong Coulomb repulsion. This case is as illustrated in Fig. 5.2A. Only when a level of the island lies near μ_s and μ_d, current can flow as shown in Fig. 5.2B. The behavior is called a Coulomb blockade, and it leads to an oscillation in the conductance as a function of gate voltage. See Fig. 5.2C. The tunneling of electrons occurs one at a time because the $(N_e + 1)$ state can be occupied by one electron due to the Pauli's exclusion principle. This is why Coulomb blockade behavior is considered as a manifestation of the single charge tunneling. The conduction occurs via the single charge tunneling. The Coulomb peaks are broadened by thermal energy $k_B T$. The relation between the oscillation period ΔV_g and the required energy for the single charge tunneling ΔE_{add} is $e\alpha_g \Delta V_g = \Delta E_{add} - \Delta_N$. If the island size is large enough and the quantum confinement is negligible, the equation can be simplified as $e\alpha_g \Delta V_g = \Delta E_{add}$. It now shows the definition of the gate influence factor, ratio of total energy of the system to the single electron charging energy of the gate $e\Delta V_g$.

alt-text: Fig. 5.2

Fig. 5.2
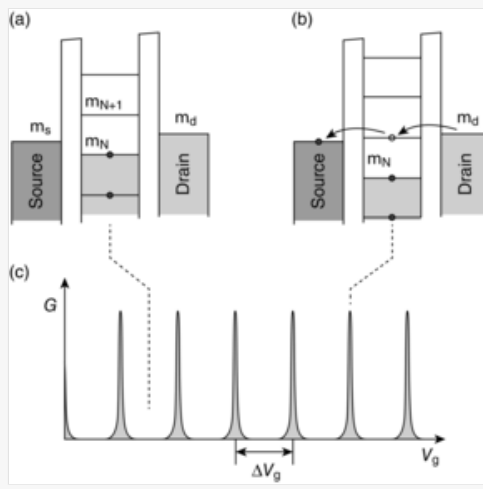
(A, B) A schematic diagram of a single charge tunneling behavior in an SET. When the chemical potentials of the source and drain electrodes lie in the gap between the levels of N_e electrons and $(N_e + 1)$ electrons, conduction is blocked (A). When the level aligns with the Fermi energies of source and drain, electrons can tunnel one at a time (B). (C) Coulomb oscillation of G as a function of V_g.
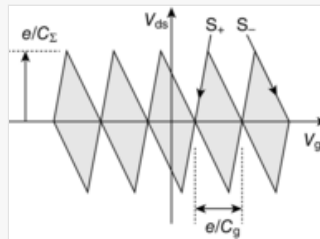
5.2.2 Coulomb diamonds

Q6 The Coulomb oscillation is also affected by changing the source-drain bias voltage (Fig. 5.3). The energy change after one electron tunnels from the source electrode to the island (ΔE_s) and from the island to the drain electrodes (ΔE_d) with a finite V_{ds} is

$$\Delta E_s = \frac{e}{C_\Sigma} \left[e \left(N + \frac{1}{2} \right) - V_{ds} \left(C_s + \frac{C_g}{2} \right) + C_g V_g \right],$$ (5.2)

$$\Delta E_d = \frac{e}{C_\Sigma} \left[-e \left(N - \frac{1}{2} \right) - V_{ds} \left(C_d + \frac{C_g}{2} \right) - C_g V_g \right].$$ (5.3)

alt-text: Fig. 5.3

Fig. 5.3

Coulomb diamond structures. *Gray diamonds* are the regions where the conductance is suppressed.

Details of the calculation can be found in references [3, 4]. Electrons can tunnel from source to drain when both the energies are negative assuming zero temperature, $\Delta E_s < 0$ and $\Delta E_d < 0$, and otherwise the conductance is zero. This

Q7 leads to a condition in which the conductance is blocked regime, which is

$$e \left(N - \frac{1}{2} \right) < C_g V_{ds} + \left(C_s + \frac{1}{2} C_g \right) V_g < e \left(N + \frac{1}{2} \right),$$

$$e\left(N - \frac{1}{2}\right) < C_g V_{ds} - \left(C_d + \frac{1}{2}C_g\right)V_g < e\left(N + \frac{1}{2}\right). \tag{5.4}$$

When projected in a $V_g - V_{ds}$ plane this condition defines a regime where the conduction is prohibited and regime shows diamond like structures, so-called Coulomb diamonds[Instruction: (Fig. 5.3)]. Conductance of a SET measured as a function of V_g and V_{ds} is zero in this regime and shows Coulomb peaks at the diamond edges. From the positive and negative slopes of the edges, C_d and C_s values can be estimated according to Eq. (5.3).

5.3 Electrical properties of graphene

5.3.1 Electronic structure of graphene

Graphene is the basic building block of graphite and carbon-based nanomaterials such as carbon nanotubes. It is a purely two-dimensional system because it is composed of a single layer of carbon atoms, which make the honeycomb lattice. It shows unconventional properties such as high thermal conductivity [5], high and nearly equal mobilities at room temperature for both electron and hole conduction up to 200,000 cm^2 V^{-1} s^{-1} [6–8], and ballistic transport in micrometer length scale [6–8]. These properties stem from the massless nature of the charge carriers due to the linear energy dispersion relation [9–12] and make graphene a promising candidate for nanoelectronic devices.
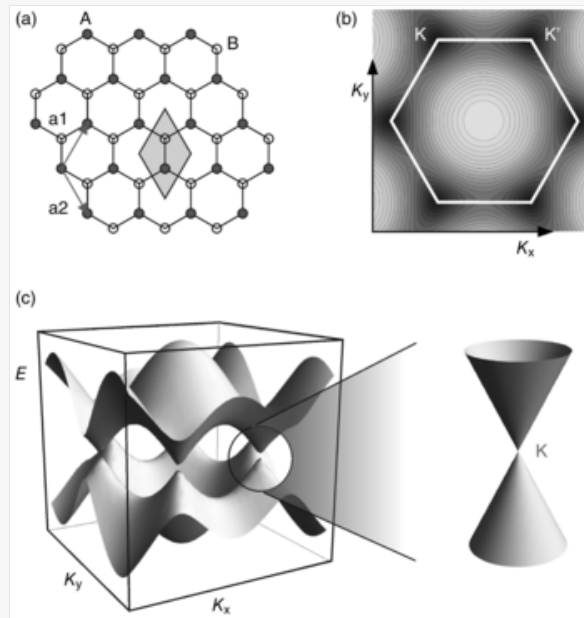
The lattice structure of graphene as well as its band structure is shown in Fig. 5.4a. The lattice possesses two sublattices denoted by A and B, and they give a rise to the valley degeneracy (or often termed as pseudospin) in addition to the trivial spin degeneracy. Near the Dirac point *chirality* is defined in regard to this pseudospin associated with the two components of the wave function [9]. Ignoring the second order hopping, the energy dispersion relation is calculated as

$$E\left(k_x, k_y\right) = \pm\gamma_1\sqrt{1 + 4\cos\left(\frac{\sqrt{3}ak_y}{2}\right)\cos\left(\frac{ak_x}{2}\right) + 4\cos^2\left(\frac{ak_x}{2}\right)}, \tag{5.5}$$

where k_x, k_y are the components of two-dimensional momentum, γ_1 is the nearest-neighbor hopping energy and a is the lattice constant, $a = \sqrt{3}a_0$, where a_0 is the C—C distance of the graphene honeycomb lattice [9, 11]. The band structure is shown in Fig. 5.4b and c. A simplified form of the dispersion relation near zero energy is, $E(q) \approx \pm v_F q$, where v_F is the Fermi velocity ($\sim 1 \times 10^8$ cm/s) and q is the relative moment to Dirac points (K or K'). This linear dispersion is depicted in Fig. 5.4c. Due to this linear dispersion relation near zero energy the charge carriers follow the Dirac equation rather than Schrödinger equation. The Dirac equation is given by $-iv_F\vec{\sigma}\cdot\nabla\psi\left(\vec{r}\right) = E\psi\left(\vec{r}\right)$, where $\vec{\sigma}$ is the Pauli matrix and $\psi\left(\vec{r}\right)$ is the particle's wavefunction.

alt-text: Fig. 5.4

Fig. 5.4

(a) Atomic structure of graphene. *Gray diamond* shows the unit cell of the lattice. A and B denote sublattices. (b, c) Band structure of graphene. *White hexagon* denotes the first Brillouin zone in (b). The *three-dimensional image* shows both the conduction and valence bands, which touch at K and K' points.

5.3.2 Transport properties of graphene

Transport measurement usually deals with low energies. In transport measurements, graphene linear dispersion relation therefore holds. In conventional semiconductors, particles follow a parabolic band, and the density of states (DOS) stays constant regardless of energy. However, in graphene with linear band, the DOS increases linearly with increasing the absolute value of energy (Fig. 5.5). The conduction and valence bands touch each other only at the Dirac points and thus Fermi surface vanishes at zero energy. Despite the zero DOS, there is no band gap at zero energy.

alt-text: Fig. 5.5

Fig. 5.5
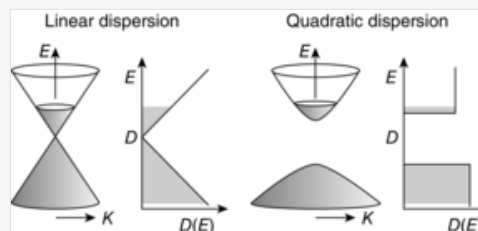
Density of states as a function of energy $D(E)$ for particles with linear and quadratic dispersion.

The behavior of DOS can be observed via transport measurement on graphene transistors. The upper inset of Fig. 5.6 shows a scanning tunneling microscope image of the suspended graphene device. The lower two insets of Fig. 5.6 show optical images of the device exfoliated from highly oriented pyrolytic graphite (HOPG) that is transferred onto an Si substrate (left-hand side) and the device is grown on a metal substrate and transferred onto Si (right-hand side). The Si chips are covered by a thermally grown oxide layer with a thickness of around 300 nm. The oxide layer makes monolayer graphene visible [13] as well as acting as a gate dielectric. The highly doped Si is used as a backgate to modulate the charge carrier density (n) in graphene. For the 300 nm thick SiO_2, the carrier density can be estimated by the relation $n = \alpha V_{bg}$, where the gate efficiency factor $\alpha \approx 7.2 \times 10^{10}$ cm^{-2} V^{-1} [14]. Fig. 5.6 shows the resistance (R) as a function of the backgate voltage (V_{bg}), which is often referred to as transfer characteristics. Due to the vanishing DOS near the "charge neutral point," a resistance peak appears. The roughly symmetric transfer curves demonstrate the electron-hole symmetry.
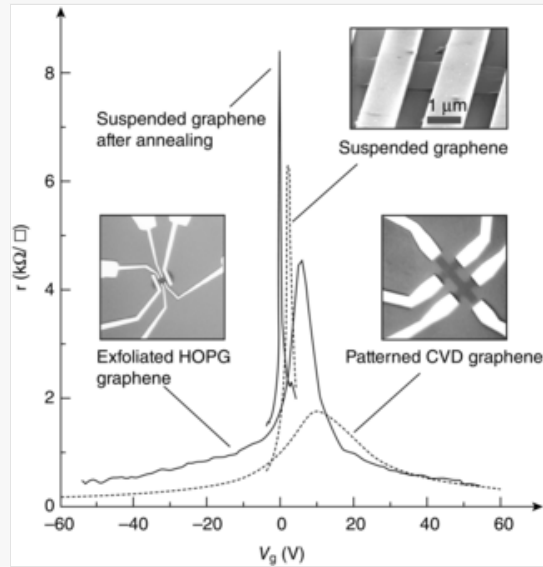
Transfer characteristics measured on a patterned CVD graphene, a graphene flake exfoliated from HOPG, and a suspended graphene device before and after current annealing. *Insets* show the representative images of the devices (an SEM image on the top and optical microscopy images). The density inhomogeneity obtained from the full width of half maximum of each peak is 1.8×10^{12}, 5×10^{11}, 1.7×10^{11}, and 6×10^{10} cm^{-2}, for the patterned CVD graphene, the exfoliated HOPG graphene, the suspended graphene and the suspended graphene after annealing, respectively.

Here one should note that the charge neutrality point does not necessarily correspond to the Dirac point of the band. The explanation is as follows. One cannot expect a system without disorder in nature. The origin of disorder in graphene can be structural defects [15–18], charged impurities [19–21], corrugation [22, 23], ripples [24], substrate roughness [25], and so forth, or it can be a combination of these. Regardless of their origin, disorders induce a potential variation along the sample as seen in Fig. 5.7. Following the disordered potential landscape, the local band structure varies. As a consequence of the disordered potential and the gapless nature of the graphene band, when the Fermi energy (E_F) is near the charge neutral point, both regions where the charge carriers are dominated by electrons and holes appear. This is a unique phenomenon of graphene, the so-called electron-hole puddles formation [26], whereas density puddles with either positive or negative charges are only observed in conventional semiconductor 2DESs. Due to the electron-hole puddles one may expect a very high resistance near the charge neutral point. However, the puddle edges do not produce a clear boundary condition because the charges are not totally bound in a single puddle due to Klein tunneling [27, 28]. As a result, a finite resistance peak appears. The full-width-at-half maximum (FWHM) of the peak in an R-n curve is a rough estimation of the density inhomogeneity (Δn_d). In Fig. 5.6, graphene grown by chemical vapor deposition (CVD) shows a much larger disordered density ($\Delta n_d \cong 1.8 \times 10^{12}$ cm^{-2}) than exfoliated graphene from highly oriented pyrolytic graphite (HOPG) ($\Delta n_d \cong 5 \times 10^{11}$ cm^{-2}). Because the substrate roughness or embedded charges inside the SiO$_2$ substrate are the main source of the disorder in graphene transistors [26], when the substrate is removed and graphene device is suspended [29, 30], the resistance peak becomes very narrow showing low $\Delta n_d \cong 6 \times 10^{10}$ cm^{-2}. Also, the resistance at the peak becomes higher as seen in Fig. 5.6.
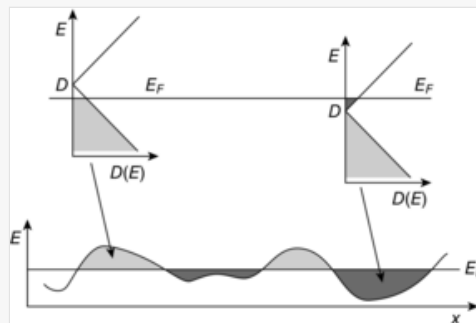
When a magnetic field is applied, the quantum Hall effect (QHE) is observed in graphene as in conventional 2DESs. However, the behavior is distinct from that of 2DESs. Conventional 2DESs have massive carriers following a parabolic band structure and as a result exhibit quantum Hall plateaus at integer filling factors (integer QHE). Graphene having the linear dispersion relation and the zero band gap, however, shows quantum Hall plateaus at Hall conductivities $\sigma_{xy} = \nu e^2/h$ for the filling factor sequence $\nu = \pm\,2, \pm\,6, \pm\,10, ...$, ignoring interactions, which is the so-called "half-integer QHE" [10, 12]. Here, h is the Planck's constant. Note that the fourfold degeneracy with spin and valley symmetries is taken into account. The QHE in graphene is shown in Fig. 5.8. The unique half-integer QHE is due to the zero energy Landau level (LL) degeneracy. The LL energy in graphene is given by $E_N = \pm\,\hbar\omega_c(N + 1/2)$, where $\hbar$ is the Planck's constant over 2π, $\omega_c = eB/m^*$ is the cyclotron frequency, and N is the quantum number. Here, B is the magnetic field and m^* is the effective mass. The DOS at zero magnetic field collapse into LLs at a finite magnetic field. The LL degeneracy is $4eB/h$. The factor 4 arises from the fourfold degeneracy. However, in the lowest LL pinned at zero energy, which is by itself unusual, electrons and holes share the state and both are half degenerate. When disorder becomes weaker, other more fragile QH states induced by interactions emerge. For instance, spontaneous symmetry breaking gives rise to the states with twofold symmetry (spin or pseudospin) at $\nu = 0, \pm\,4, \pm\,8, ...$, as well as the fully broken symmetry states at $\nu = \pm\,1, \pm\,3, ...$ [31–36]. Also fractional quantum Hall states appear as a result of the formation of composite quasiparticles [29, 30, 37–39].

alt-text: Fig. 5.8

Fig. 5.8
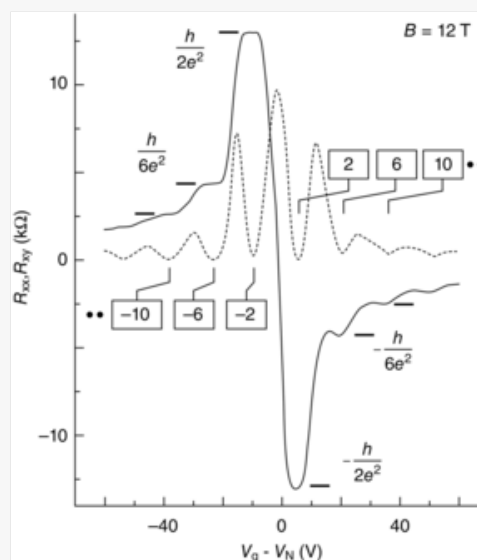
Typical quantum Hall behavior of graphene. Longitudinal resistance (R_{xx}) and Hall resistance (R_{xy}) traces measured at 12 T are plotted as a function of $V_g - V_N$, where V_N is the voltage of charge neutrality.

5.4 Single charge tunneling in graphene

When electrons in graphene are confined in one-dimension (graphene nanoribbons) or in two-dimension (graphene quantum dots), single charge tunneling behavior occurs within the massless Dirac nature of particles. This will promise rich physics behind the confined Dirac particles. For the study, the advantages of graphene over other nanomaterials such as carbon nanotubes (CNTs) or semiconductor nanowires are its two-dimensionality and the fact that it can be patterned by a lithographic process followed by etching. Such a process is easily accessible because it is based on the conventional top-down approach. The quantum confinement effect in graphene nanoribbons and in graphene single electron transistors has been investigated in experiments as well as in theoretical studies. They will be reviewed in this section.

5.4.1 Band gap opening in graphene

One of the most attractive electronic applications of graphene is field-effect transistors because it exhibits excellent electrical properties such as very high carrier mobility with an electron-hole symmetry [10, 14, 40, 41] and ballistic

transport in a large length scale of microns [42]. Moreover, it shows a high thermal conductivity that exceeds those of diamond and graphite [43] so it may be used for integrated devices with a much lower heat dissipation compared to the conventional silicon-based devices. However, we have a serious problem that graphene has only a zero-band gap. The off-state current is not totally suppressed near the charge neutral point. This is because there are always charge carriers near the charge neutral point, electron-hole puddles, due to the presence of disorders. Martin et al. have well demonstrated this localized phenomena of the electron-hole puddles in graphene [26].

Opening a band gap in graphene is, therefore, one of the key issues in the quest to achieve a high performance of graphene electronic devices. Several ways to open a band gap in graphene have been proposed: graphene superlattices, graphene nanomeshes, biased bilayer graphene, and graphene nanoribbons. The approach of graphene superlattices is to break the valley symmetry by introducing another periodicity in addition to the honeycomb lattice. There have been suggestions to produce these graphene superlattices, for example, the periodic ripples often found in graphene grown **Q12** on metal substrates [44], antidot lattices [45–47], a periodic potential [48], patterned hydrogen adsorption [49], substrate-induced superlattice on BN [50], lithographic patterning [51, 52], and so forth. Graphene nanomesh, an array of graphene nanoribbons, exhibits an effective band gap in transport. The mesh structure is obtained via a plasma etching process on patterned masking layers such as membranes, block copolymer layers and nanoimprinted layers [53–56]. Such a band gap opening was also observed in amorphous carbon nanomesh synthesized directly from phase-separated polymer blends [57]. Graphene nanomesh has been also studied as a promising material for the thermoelectric devices because it significantly reduces the thermal conductivity when the porosity is controlled [58, 59]. An energy gap feasible for the field-effect devices, say, more than 0.1 eV, has been achieved in biased bilayer graphene. In order to induce an asymmetry of the on-site energies in the top and bottom layers [60–62], researchers have used molecular doping on graphene grown by thermal decomposition of SiC [63], a dual-gate structure fabricated on an exfoliated bilayer graphene flake [64–67], or dual molecular doping on both the top and the bottom of a bilayer graphene flake [68].

5.4.2 Graphene nanoribbons

Another approach for the band gap opening is to spatially confine the electron wave functions in graphene. For instance, one can shrink the width of a graphene field-effect device in the nanometer scale, which results in graphene nanoribbons. They show metallic or semiconducting behaviors depending on their width and atomic structure at the edge. This is analogous to carbon nanotubes, where the boundary condition is determined by the rolling direction (chiral vector) of a graphene sheet, while in graphene nanoribbons two edges determine the boundary condition. Graphene nanoribbons have been intensively studied as another route toward the field-effect transistor application [69–78] because they exhibit a tunable band gap. Graphene nanoribbons serve not only as the high performance field-effect transistors but also, in the respect of quantum mechanics, as a system for a fundamental study on single charge tunneling behavior, in particular that of massless Dirac particles. When a nanoribbon or a nanoconstriction interconnects two metallic systems (either metal electrodes or bulk graphene flakes), the energy gap (or the different energy gaps distributed along the translational direction) of the constriction acts as a tunnel barrier, which is essential for the single charge tunneling.

The electronic structure of the graphene nanoribbons [79–82] was theoretically studied much earlier (in 1996) than the exfoliation of the one-atom-thick sheet, "graphene" (in 2004) [14]. The basic electronic properties of graphene nanoribbons were even then discovered by calculations using a tight binding model. Fujita et al. [80] showed the band structures of graphene nanoribbons with zigzag edges and armchair edges. Here, they found that for graphene with zigzag edges, a peculiar edge ferromagnetism is present with an antiparallel spin orientation between the two opposite edges and for graphene with armchair edges, a band gap appears. Nakada et al. [81] and Ezawa [79] revealed that graphene nanoribbon with armchair edges has an energy gap Δ that is tunable by changing the width w. Here, w usually scales in the units of the number of dimer lines perpendicular to the translational direction of the ribbon, N_a and N_z for the graphene nanoribbons with armchair edges and with zigzag edges, respectively (see Fig. 5.9). Depending on the boundary conditions, if some of the one-dimensional modes cross the Dirac point, and then the ribbon shows metallic behavior, but it is otherwise semiconducting with a finite energy gap. When $N_a = 3p$ or $3p + 1$, graphene with **Q13** armchair edges shows a band gap while it is metallic when $N_a = 3p + 2$, where p is an positive integer. Nanoribbons with the zigzag edge on the other hand always exhibit a flat band at zero energy regardless of the ribbon width as shown in Fig. 5.10. However, according to a recent ab initio calculation [83], even for graphene nanoribbons with

zigzag edges, gaps appear because of a staggered sublattice potential on the hexagonal lattice due to edge magnetization (see Fig. 5.11).
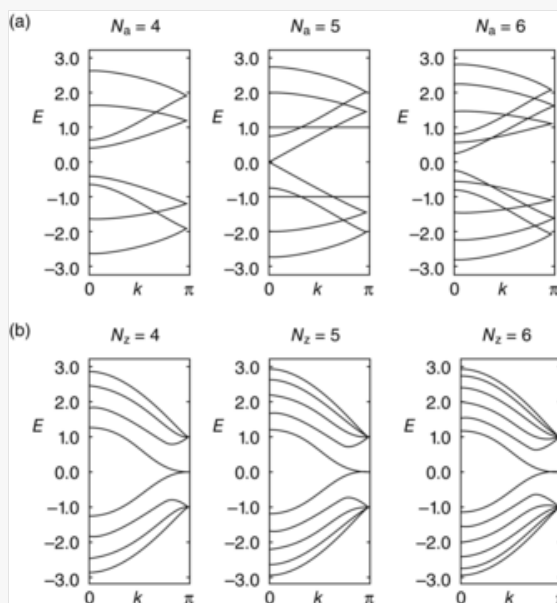
alt-text: Fig. 5.9

Fig. 5.9
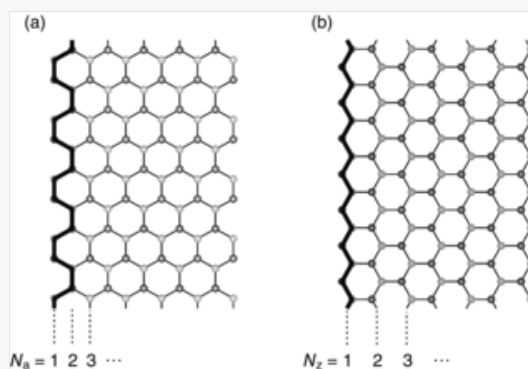
The atomic structures of an armchair nanoribbon ($N_a = 11$) (A) and a zigzag ribbon ($N_z = 7$) (B). *Dark gray* and *light gray dots* indicate the sublattices. The edge sites are indicated by the *thick lines*.
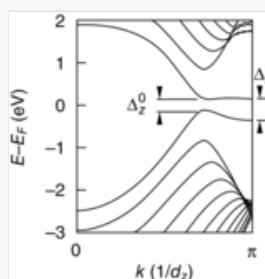
alt-text: Fig. 5.10

Fig. 5.10

Band structures of armchair (A) and zigzag ribbons (B) of various widths calculated by a tight binding model.
Modified from K. Nakada, M. Fujita, G. Dresselhaus, M.S. Dresselhaus, Edge state in graphene ribbons: nanometer size effect and edge shape dependence, Phys. Rev. B 54 (1996) 17954–17961.

alt-text: Fig. 5.11

Fig. 5.11

It is not yet possible to experimentally fabricate a graphene nanoribbons with clear edges either of armchair or of zigzag orientation only (Fig. 5.12). The edges are usually rough, containing both the armchair and zigzag orientations not only in patterned nanoribbons but also in exfoliated flakes. See, for instance [84]. There are several ways to fabricate graphene nanoribbons. A common approach is to reduce the size of graphene by e-beam lithography and a plasma etching technique [85–87]. For this approach, graphene is often obtained by mechanical exfoliation from crystals of natural graphite or HOPG using a sticky tape [14] and deposited on a silicon substrate with an about 300 nm-thick thermally grown oxide, which make monolayer graphene visible in an optical microscope due to an increased optical path and the notable opacity of graphene [13]. The transferred flakes are identified by an optical microscope. An e-beam resist is spin-coated on the SiO_2 substrate with the transferred graphene flakes. An appropriate etching pattern is drawn on the resist on top of graphene flakes by e-beam lithography, and the exposed resist pattern is developed by a chemical solvent. Now, a part of the graphene flake is exposed and the chip is subjected to a reactive ion etching (RIE) chamber for the O_2 or Ar plasma etching of the part. After removal of the resist, the patterned graphene nanoribbons or nanoconstrictions are prepared and the electrical contacts to the devices are made by further processes of e-beam lithography and metalization. The energy gap in graphene nanoribbons shows an inversely proportional behavior to the width of the ribbons as reported in [86], who found that Δ [eV] $\approx 0.2/(w[\text{nm}] - 16[\text{nm}])$ (Fig. 5.12). The energy gap, for instance, 0.1 eV, can be obtained in graphene nanoribbon with $w \sim 18$ nm, say, less than 20 nm. Though the procedure is quite common and reliable, it is not suitable for definition of atomically clear edge structures due to the anisotropic nature of plasma etching process and a bad etch selectivity of graphene to the resist mask under the plasma.

alt-text: Fig. 5.12
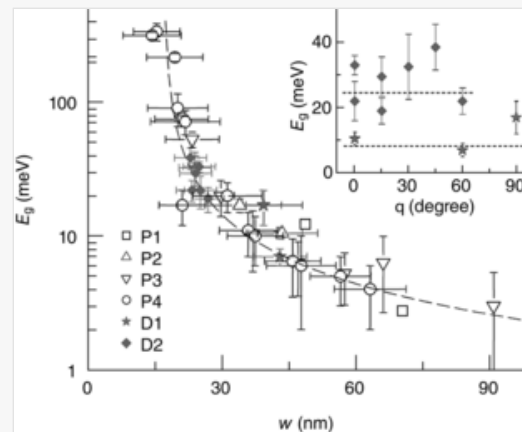
Fig. 5.12

Atomic force microscope (A) and scanning electron microscope images (B, C) of graphene nanoribbon devices. (D-F) Temperature dependent conductance of the ribbons with various widths. (G) The energy gap as a function of the width of devices.

Modified from M.Y. Han, B. Özyilmaz, Y. Zhang, P. Kim, Energy band-gap engineering of graphene nanoribbons, Phys. Rev. Lett. 98 (2007) 206805.

Although coherent transport is expected through a graphene nanoribbon [88, 89], it is not yet possible to fabricate clear edges on graphene nanoribbons (Fig. 5.13). Instead, at low temperatures, the gate-dependent behavior conductance (G) is often cluttered by oscillations or fluctuations [90–92]. They may be due to the network of graphene quantum dots (QDs) and/or the rough edge structures. Even Coulomb diamond-like structures are quite commonly observed in graphene nanoribbons [90, 91, 93]. However, nanoribbons with the disordered edge (mixture of zigzag and armchair

edges) have shown the conductance quantization sequence of the integer multiples of $2e^2/h$ due to the ballistic charges of graphene and the valley degeneracy lifting [92, 94].

Fig. 5.13
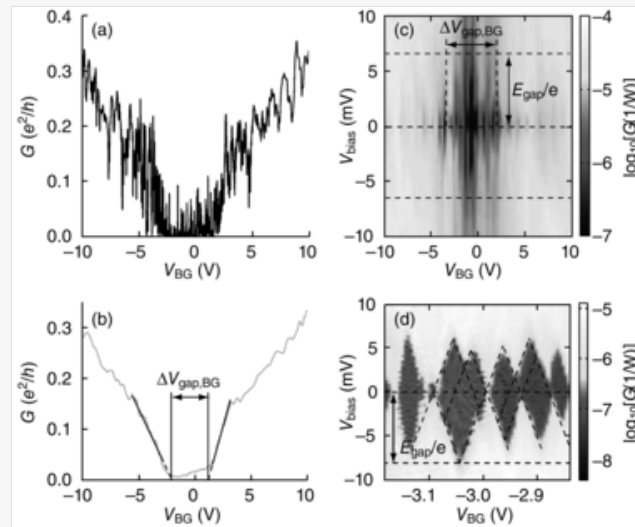
(A) Conductance as a function of V_g. (B) A smoothed trace of the curve in (A). (C) Stability diagram of a graphene nanoribbon device. (D) Zoom of the plot in (C).

Modified from F. Molitor, A. Jacobsen, C. Stampfer, J. Güttinger, T. Ihn, K. Ensslin, Transport gap in side-gated graphene constrictions, Phys. Rev. B 79 (2009) 075426.

A more promising way to control the edge is based on the carbo-thermal reduction of SiO_2 to SiO in argon environment at around 700°C [95]. The carbon atoms at the edge of graphene are used for the process and the flake edges aligned in the crystallographic direction (Fig. 5.14). A Raman spectroscopy study confirmed the graphene edge orientations [84]. A similar result was obtained by a hydrogen plasma etching [96], a gas-phase chemistry etching process [97] or by plasma etching using nanospheres as a mask [98]. With these methods, long graphene nanoribbon transistors with controlled edges were fabricated [96–100]. However, single charge tunneling behavior using the edge-controlled nanoribbons or constrictions has not yet been reported.

Fig. 5.14
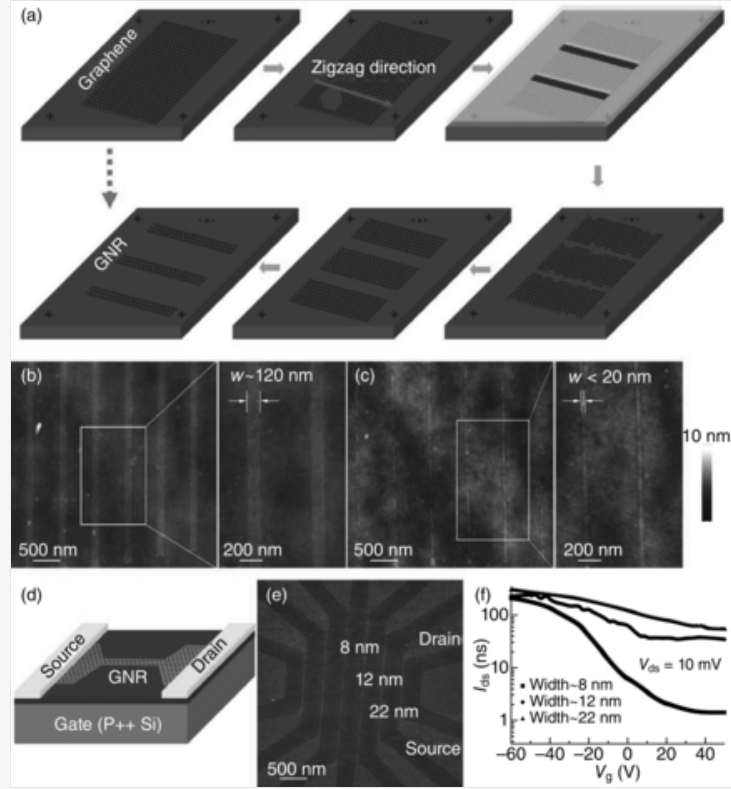
Graphene nanoribbons fabricated by anisotropic etching.

Modified from R. Yang, L.C. Zhang, Y. Wang, Z.W. Shi, D.X. Shi, H.J. Gao, E.G. Wang, G.Y. Zhang, An anisotropic etching effect in the graphene basal plane, Adv. Mater. 22 (2010) 4014–4019.

5.4.3 Graphene single electron transistors

Graphene SETs can be defined by isolating a part of a graphene flake and connecting it with two constrictions (or nanoribbons) on the opposite sides, which serve as the source and drain capacitors. A side gate structure can be patterned on graphene, or Si backgate can also be used to modulate the electrostatic energy of the island. So far, in order to pattern the SET structure on graphene, researchers often used the plasma etching technique. The basic structure of graphene SETs is the same as conventional SETs based on metals or semiconductors. However, there is a clear distinction. Due to the massless nature of the charges in the system, the quantum confinement is different from that for conventional SETs, where the charges obey the massive parabolic dispersion relation.

Here we consider the quantum confinement energy, which becomes important when the size of the island is small enough, that is, it is considered as a QD. For massive carriers for instance in 2DES, the quantum confinement energy of an island is given from the two-dimensional box problem by $\Delta_N \approx h^2/(8m_e d^2)$, where m_e is the effective mass and d is the diameter of the island. It shows Δ_N is proportional to $1/d^2$. However, a different spectrum is applied for graphene SETs with massless charge carriers as, $\Delta_N \approx v_F h/(2d)$. Here Δ_N is inversely proportional to d. The $1/d$ dependence of the quantum confinement energy for a graphene SET has been demonstrated by [101]. They have also found that the oscillation period ΔV_g varies randomly (not showing the even-odd sequence due to the spin degeneracy of the massive carriers), and the variation of the chaotic $\delta(\Delta V_g)$ is larger than typical variations observed in nongraphene QDs by orders of magnitude (see Fig. 5.15). Furthermore, $\delta(\Delta V_g)$ becomes notably broader with decreasing d approximately following $\delta(\Delta V_g) \propto 1/d^2$. Such a "Dirac billiard" behavior raises the importance of the shape of the graphene QD for the behavior of the single charge tunneling in the system ~~(Fig. 5.16)~~. According to a theoretical calculation [102], regular-shaped (disk) graphene QDs show sharp resonances, which reduces the effective gated region, but the irregular-shaped (stadium) QDs cannot support bound states due to chaotic dynamics. Irregular Coulomb oscillation has been observed by others in a normal SET structure with patterned island [103], and Coulomb oscillation behaviors in nanoconstrictions [91, 104]. More studies are needed because a regular ΔV_g has also been observed in a normal SETs

[105, 106] (Fig. 5.16) or in a direct measurement on compressible QDs in quantum Hall regime using scanning tunneling microscopy (STM), where they observed the fourfold periodicity due to the spin and valley degeneracies [107]. In addition to the ground state Coulomb diamonds, the excited states and phenomena in a double QD system have also been revealed in experiments [103, 108, 109]. The coupling of the mechanical modes and single electron tunneling were observed in graphene mechanical resonators, which causes a shift of a resonance frequency larger than 100 kHz [110]. In bilayer graphene, a nanoscale circular p-n junction generated by the bias voltages of an STM tip and the backgate, where the confined states (of massive Dirac Femions) were visualized via STM technique [111]. Despite the intensive studies, the interesting physics behind the confined massless particles are largely unexplored. For instance, it would be an intriguing experiment if one fabricates the SET with the edge-controlled constrictions using crystallographic etching or even with a hexagonal-shaped graphene island as described in Section 5.4.1. Also, controlled spin states using specific edges will provide an insight for a spin qubits where a long-distance coupling is possible [112].

Q17
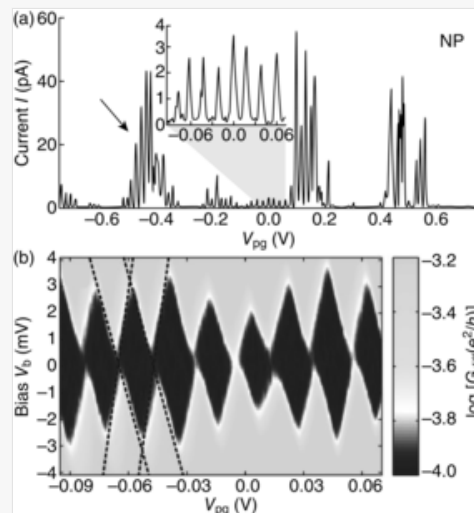
---

alt-text: Fig. 5.15

Fig. 5.15
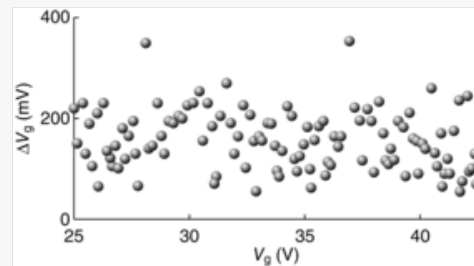
Separation of nearest-neighbor peaks at zero bias voltage (ΔV_g) measured in a graphene quantum dot. The peak spacing shows a large variation (a factor of 5 or more).
From L.A. Ponomarenko, F. Schedin, M.I. Katsnelson, R. Yang, E.W. Hill, K.S. Novoselov, A.K. Geim, Chaotic Dirac billiard in graphene quantum dots, Science 320 (2008) 356–358.

---

alt-text: Fig. 5.16

Fig. 5.16

Source-drain current as a function of the gate voltage and Coulomb *diamond structures*.
From C. Stampfer, E. Schurtenberger, F. Molitor, J. Guettinger, T. Ihn, K. Ensslin, Tunable graphene single electron transistor, Nano Lett. 8 (2008) 2378–2383.

5.5 Charge localization in graphene

5.5.1 Localization in the quantum Hall regime

Localization of charges in the quantum Hall regime, which gives rise to the quantum Hall plateaus, has been found to occur within the boundaries of Coulomb blockade physics [2, 113]. For the charge confinement, the insulating barriers of incompressible strips play an important role. As shown in Section 5.3.2, a disordered potential landscape in graphene induces a density profile along the sample. The carriers are redistributed to flatten the disordered potential as shown in Fig. 5.17. This linear screening is not valid when a perpendicular magnetic field is applied though. In some regions, the level degeneracy is completely filled as n increases, and the carriers cannot screen out the disordered potential in these regions. Due to the gap between the LLs, carriers can no longer be injected, that is, the regions become totally incompressible. The incompressible regions serve as insulating barriers to enclose the compressible dots. The charges coming into the compressible QDs are governed by Coulomb blockade physics. Every charging event occurs by one electron (or hole) at a time into the discrete levels of the QDs. This leads to a sudden jump in the local compressibility ($dn/d\mu$), where μ is the chemical potential. At higher B field, the same density profile appears at accordingly higher n because the LL degeneracy is proportional to B (eB/h). The compressibility spikes produce lines parallel to specific filling factors as shown in Fig. 5.17. The presence of the compressible QDs in the QH regime has been demonstrated by a direct transport measurement on the dots using an STM tip [107].


alt-text: Fig. 5.17

Fig. 5.17
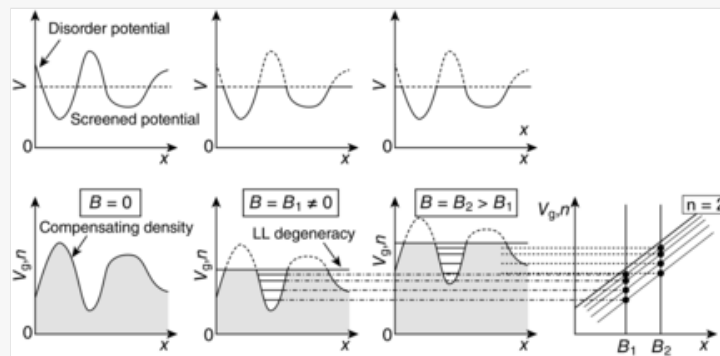
Schematics of the compressible QD formation at high magnetic field.

5.5.2 Compressible quantum dots in the quantum Hall regime

The influence of the compressible QDs on macroscopic conductance of graphene device has recently been investigated by magnetotransport measurements of conductance fluctuations [114]. Conductance curves as a function of V_{bg} at high magnetic fields often possess fluctuations, which clutter the main conductance quantization behavior. However, these fluctuations are found to be a manifestation of charge localization. Although the local process is not shown in mesoscopic transport due to the averaging, the fluctuations can reflect the single charge tunneling that occurs locally into the compressible QDs. Conductance as a function of n at 15 T is shown in Fig. 5.18A. In addition to the quantized steps and the signatures of quantization, there are fluctuations, which are reproducible for repeated measurements. These fluctuations are more pronounced if one measures transconductance g_m. Here, an ac modulation δV_{bg} is applied to the backgate, only the ac component of the source-drain current δI_{ds} is measured, and $g_m = \delta I_{ds}/\delta V_{bg}$. Both measurements were done with a dc-voltage bias of $V_{ds} = 500$ μV. The frequency of δV_{bg} was 433 Hz, and its root-meansquare amplitude was 10 mV. Insets show the schematics of the measurements.


alt-text: Fig. 5.18

Fig. 5.18
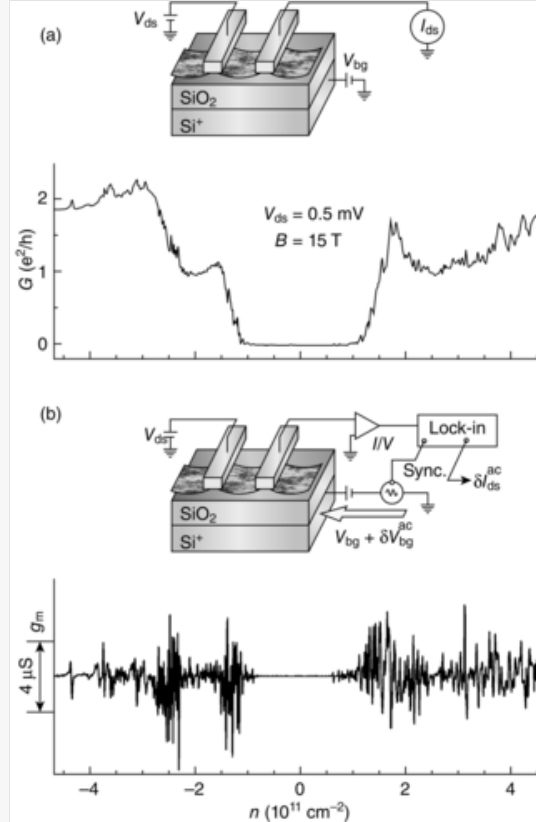
Conductance (A) and transconductance (B) curves measured at $B = 15$ T. Diagrams show the measurement schematics.
From [114] D.S. Lee, V. Skakalova, R.T. Weitz, J.H. Smet, K. von Klitzing, Transconductance fluctuations as a probe for interaction-induced quantum Hall states in graphene, Phys. Rev. Lett. 109 (2012) 056602.

The same backgate sweep was repeated for different magnetic fields. The result is plotted in a [Instruction: 1. intead of "color rendition" should be "grayscale rendition"]color rendition in a (n, B)-plane. See Fig. 5.19A. There are many line features and they are classified into groups in which lines are parallel to each other. The lines in a group run parallel to a certain filling factor line. The lines parallel to $\nu = \pm 2$ are the most strong and sharp as the filling factor 2 is most profound because of the largest gap between $N = 0$ and $N = 1$ LLs. Also, $\nu = 6$-line can be discerned, which is another half-integer filling factor. Surprisingly, more fragile broken symmetry states and fractional quantum Hall states can be clearly seen in the fluctuation map, ~~while~~whereas, in a similar map of conductance, such states are invisible or ~~only~~ seen only as faint signatures ~~if visible~~. Details can be found in Ref. [114].

alt-text: Fig. 5.19

Fig. 5.19
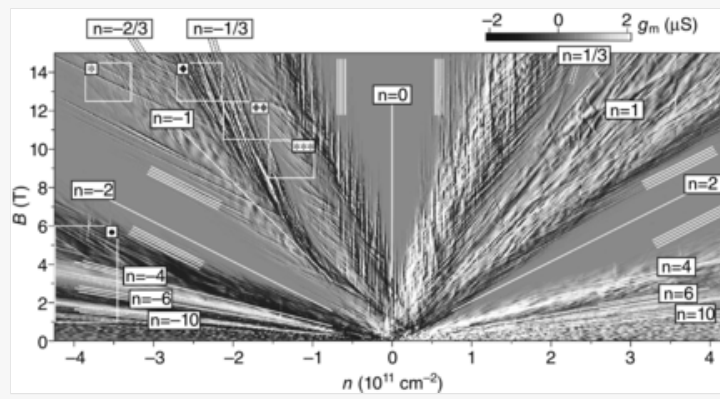
The [Instruction: ...color... -> ...grayscale...]color rendition with the line features resembles the local compressibility map measured on graphene [113] as well as earlier on GaAs 2DESs [2] using a scanning SET. Thus, it is natural to associate the conductance fluctuations with the compressible spike lines. Far from the complete filling of the level degeneracy, the linear screening holds. As one increases n by modulation of the backgate, compressible quantum dots emerge as described in Section 5.5.1. Incompressible strips play a role to isolate the dots. As illustrated in Fig. 5.20, conducting channels are always present near the sample edge due to the edge potential. Current can flow through these edge states. During modulation of n, the compressible spikes may emerge for some dots due to the Coulomb blockade allowing charging of the dots. Accordingly, additional transport channels through the network of the dots may be turned on, off, or their path is altered. At every compressible spike the charging give rises to a fluctuation of the source-drain current. The same fluctuation behavior would occur at the same deviation of n from complete filling even at a different magnetic field. As a consequence, the conductance fluctuation peaks or valleys run parallel to the filling factor lines in the (n, B)-plane. It should be noted that the line features of the conductance fluctuations have already been discovered in GaAs 2DESs [115] and recently in graphene [116, 117]. They just measured the resistance and the results showed only the lines parallel to the single particle states, half-integer QH states in graphene, and integer QH states in GaAs, respectively. In the transconductance measurement, using the lock-in technique reveals the presence of more fragile interaction induced states of broken symmetry states and fractional quantum Hall states [114]. For instance, $\nu = 0$ and $\nu = 1$ lines for broken symmetry states and a fractional filling factor ($\nu = 1/3$) lines are also found in the color rendition of Fig. 5.19A.

alt-text: Fig. 5.20

Fig. 5.20
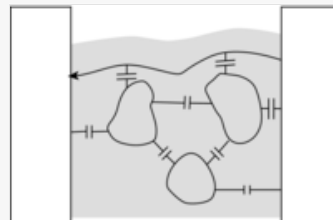
Schematic illustration of compressible quantum dots and edge channels in a graphene device.

In order to visualize the strength of the fluctuations lines as well as to determine the filling factor of the lines we transform the data set in a window into a correlation spectrum as a function of filling factor, $C(\nu)$, which shows how much the data along a certain slope in the (n, B)-plane are correlated and thus how distinctively they make the line with the slope. A schematic illustration of the calculation is shown in Fig. 5.21. Here, the data set of g_m as a function of n and B can be regarded as a matrix, $D(n, B)$. A data window is chosen in $n_{min} \leq n \leq n_{max}$ and $B_{min} \leq B \leq B_{max}$. The matrix element is then, $D_{ij} \equiv D(n_j, B_i)$. Here, n_j (B_i) is the jth (ith) element of n (B) from n_{min} (B_{min}). The correlation function as a function of filling factor is then defined as

$$C(v) = \frac{\sum_{k,l,p,q,k\neq p} D_{kl} D_{pq} \delta_v}{\sum_{k,l,p,q,k\neq p} \delta_v},$$ (5.6)

where δ_v is an allowance function defined as, $\delta_v = 1$ if $r(\theta_m) < r_a$ and $\delta_v = 0$, otherwise. Here $r(\theta_m)$ is the distance in the unit of data pixels (Δ_n and Δ_B) between the point of D_{pq} and the line crossing the point of D_{kl} with a slope, $s = \tan(\pi/2 - \theta_m)$, that is, the line for the filling factor, $v(\theta_m) = (\Phi_0/s) \cdot (\Delta_n/\Delta_B)$. Here, the denominator in Eq. (5.6) is a normalization factor. The allowance factor is chosen as $r_a = 1$. For the value of $v(\theta_m)$ parallel to the line features of the g_m peaks or deeps the summation of $D_{kl} D_{pq}$ will be larger, whereas it will be canceled out when $v(\theta_m)$ line is not parallel to the line features in the map. The analysis is shown in Fig. 5.22.
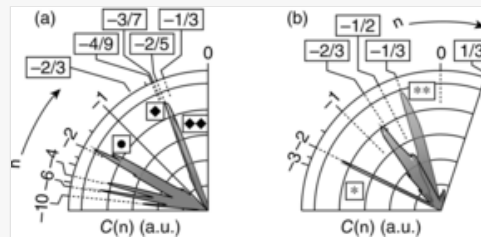

alt-text: Fig. 5.21

Fig. 5.21
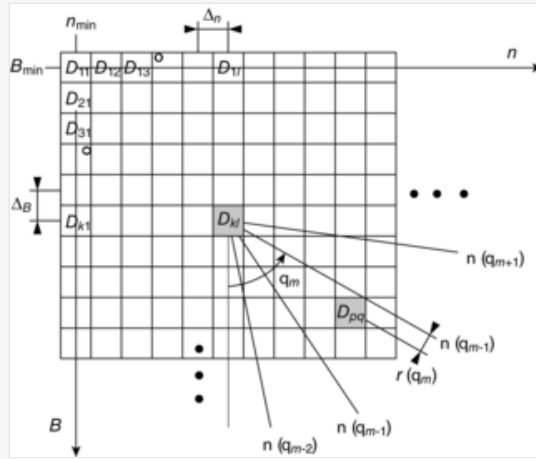
Schematic illustration of the data analysis using $C(v)$.

alt-text: Fig. 5.22

Fig. 5.22

Correlation function.
From D.S. Lee, V. Skakalova, R.T. Weitz, J.H. Smet, K. von Klitzing, Transconductance fluctuations as a probe for interaction-induced quantum Hall states in graphene, Phys. Rev. Lett. 109 (2012) 056602.

In the spectrum of $C(v)$ obtained from the data in the lower left rectangle in the color rendition of Fig. 5.19, filling factors of $v = -2, -4, -6,$ and -10. Here, $v = -4$ state is particularly interesting because it is attributed to a symmetry breaking either of spin or valley. Also, it did not appear in the conductance data [114]. Fractional quantum Hall states appear as well. $C(v)$ obtained from the data in the upper rectangular window clearly shows the filling factors $v = -1/3, -2/3$, which are the most pronounced fractional quantum Hall states in graphene. They are not seen in conductance measurement.

The compressible QD scenario described above is valid only when the nonlinear screening of the disorder potential produces compressible QDs isolated by the insulating barriers. Despite the recent observation of the single charge tunneling behavior on a compressible QD using STM tip [107] a direct transport measurement through the network of QDs is desirable for a better understanding on the influence of the network of QDs to the conductance fluctuations. It

is, however, prohibited by the presence of the edge channel in parallel to the network of QDs. A direct transport measurement on the network of QDs was however possible because the quantum Hall insulating behavior emerges at high magnetic fields. The true insulating behavior originates from the absence of the edge states due to the valley symmetry breaking for the zero energy states [35]. The differential conductance, dI_{ds}/dV_{ds}, as well as a ~~color~~ greyscale rendition of it as a function of V_{bg} and V_{ds} are shown in Fig. 5.23. The stability diagram of the differential conductance exhibits Coulomb diamond structures, which unambiguously proves the existence of the tunnel barriers, which isolate the QDs. The estimated length scale of the QDs from the diamond structures in Fig. 5.23 ranges from 160 to 400 nm, which can be regarded as the disorder length scale because the QDs formation is due to the nonlinear screening of the disorder potential. It was estimated from the diamond structures as $d^2 = 4C_g/(\pi e \alpha)$, where $C_g = C_\Sigma/\left(s_p^{-1} + s_n^{-1}\right)$ and where s_p and s_n are the positive and negative slopes of diamond structures. The disorder length scale can also be comparable to the mean free path (l_{mfp}) of the system. From the conductivity near the charge neutral point without magnetic field for our suspended sample, $3.5e^2/h$, we deduce l_{mfp} 350 nm [118], which is consistent with the length scale estimated from Coulomb diamonds. The irregularity of the diamonds can be either the result from the network of QDs or the result from the nondisk-like shape of the QDs where the chaotic resonance has been predicted [102].

alt-text: Fig. 5.23

Fig. 5.23
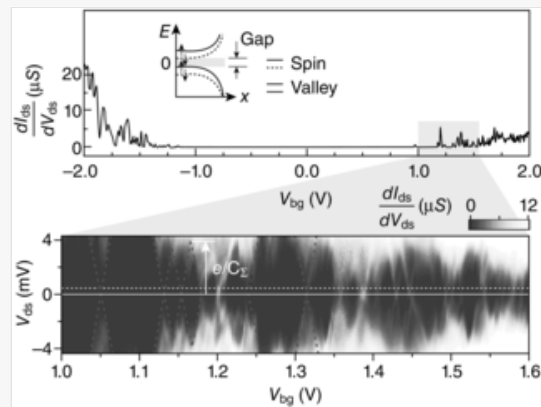
Gate dependence of $dI_{ds} = dV_{ds}$ (top) and greyscale rendition of $dI_{ds} = dV_{ds}$ as a function of V_{ds} and V_g (bottom).
From D.S. Lee, V. Skakalova, R.T. Weitz, J.H. Smet, K. von Klitzing, Transconductance fluctuations as a probe for interaction-induced quantum Hall states in graphene, Phys. Rev. Lett. 109 (2012) 056602.

5.6 Conclusion

Recent advances in the progress to control the electronic properties of graphene are significant, and they show promise for not only the applications of electronic devices such as transistors but also of quantum computational devices. However, the physics behind the single charge behavior in graphene has not yet been fully uncovered. For instance, it is not yet possible to open a band gap of graphene on a bulk scale. Attempts for the realization of single electron transistors or quantum dots of graphene by size control were reviewed in Section 5.4. In addition, the effect of single charge tunneling on mesoscopic transport and how the localization of individual charges can be captured in macroscopic devices in discussed in Section 5.5. How massless particles obey the linear dispersion relation is the key point to understand in regard to single charge transport in graphene, and such an understanding will provide insight toward the future of nanoelectronics.

References

ⓘ The corrections made in this section will be reviewed and approved by master copier.

[1]

K. von Klitzing, G. Dorda, M. Pepper, New method for high-accuracy determination of the fine-structure constant based on quantized Hall resistance, Phys. Rev. Lett. 45 (1980) 494–497.

[2] S. Ilani, J. Martin, E. Teitelbaum, J.H. Smet, D. Mahalu, V. Umansky, A. Yacoby, The microscopic nature of localization in the quantum Hall effect, Nature 427 (2004) 328–332.

[3] C.W.J. Beenakker, Theory of Coulomb-blockade oscillations in the conductance of a quantum dot, Phys. Rev. B 44 (1991) 1646–1656.

[4] H. Grabert, M.H. Devoret, Single Charge Tunneling: Coulomb Blockade Phenomena in Nanostructures, Vol. 294, Single Charge Tunneling, Coulomb Blockade Phenomena in Nanostructures NATO Adv. Sci. Inst. Ser. B, Plenum Press, New York, London, 1992.

[5] A.A. Balandin, S. Ghosh, W. Bao, I. Calizo, D. Teweldebrhan, F. Miao, C.N. Lau, Superior thermal conductivity of single-layer graphene, Nano Lett. 8 (2008) 902–907.

[6] K.I. Bolotin, K.J. Sikes, Z. Jiang, M. Klima, G. Fudenberg, J. Hone, P. Kim, H.L. Stormer, Ultrahigh electron mobility in suspended graphene, Solid State Commun. 146 (2008) 351–355.

[7] C.R. Dean, A.F. Young, I. Merici, C. Lee, L. Wang, S. Sorgenfrei, K. Watanabe, T. Taniguchi, P. Kim, K.L. Shepard, J. Hone, Boron nitride substrates for high-quality graphene electronics, Nat Nano 5 (2010) 722–726.

[8] S.V. Morozov, K.S. Novoselov, M.I. Katsnelson, F. Schedin, D.C. Elias, J.A. Jaszczak, A.K. Geim, Giant intrinsic carrier Mobilities in graphene and its bilayer, Phys. Rev. Lett. 100 (2008) 016602.

[9] A.H. Castro Neto, F. Guinea, N.M.R. Peres, K.S. Novoselov, A.K. Geim, The electronic properties of graphene, Rev. Mod. Phys. 81 (2009) 109–162.

[10] K.S. Novoselov, A.K. Geim, S.V. Morozov, D. Jiang, M.I. Katsnelson, I.V. Grigorieva, S.V. Dubonos, A.A. Firsov, Two-dimensional gas of massless Dirac fermions in graphene, Nature 438 (2005) 197–200.

[11] P.R. Wallace, The band theory of graphite, Phys. Rev. 71 (1947) 622–634.

[12] Y.B. Zhang, Y.W. Tan, H.L. Stormer, P. Kim, Experimental observation of the quantum Hall effect and Berry's phase in graphene, Nature 438 (2005) 201–204.

[13] P. Blake, E.W. Hill, A.H.C. Neto, K.S. Novoselov, D. Jiang, R. Yang, T.J. Booth, A.K. Geim, Making graphene visible, Appl. Phys. Lett. 91 (2007).

[14] K.S. Novoselov, A.K. Geim, S.V. Morozov, D. Jiang, Y. Zhang, S.V. Dubonos, I.V. Grigorieva, A.A. Firsov, Electric field effect in atomically thin carbon films, Science 306 (2004) 666–669.

[15] M.H. Gass, U. Bangert, A.L. Bleloch, P. Wang, R.R. Nair, A.K. Geim, Free-standing graphene at atomic resolution, Nat. Nano 3 (2008) 676–681.

[16] A. Hashimoto, K. Suenaga, A. Gloter, K. Urita, S. Iijima, Direct evidence for atomic defects in graphene layers, Nature 430 (2004) 870–873.

[17] J.C. Meyer, C. Kisielowski, R. Erni, M.D. Rossell, M.F. Crommie, A. Zettl, Direct imaging of lattice atoms and topological defects in graphene membranes, Nano Lett. 8 (2008) 3582–3586.

[18] J.H. Warner, M.H. Rummeli, L. Ge, T. Gemming, B. Montanari, N.M. Harrison, B. Buchner, G.A.D. Briggs, Structural transformations in graphene studied with high spatial and temporal resolution, Nat. Nanotechnol. 4 (2009) 500–504.

[19] T. Ando, Screening effect and impurity scattering in monolayer graphene, J. Phys. Soc. Jpn. 75 (2006).

[20] J.H. Chen, C. Jang, S. Adam, M.S. Fuhrer, E.D. Williams, M. Ishigami, Charged-impurity scattering in graphene, Nat. Phys. 4 (2008) 377–381.

[21] Z.H. Ni, L.A. Ponomarenko, R.R. Nair, R. Yang, S. Anissimova, I.V. Grigorieva, F. Schedin, P. Blake, Z.X. Shen, E.H. Hill, K.S. Novoselov, A.K. Geim, On resonant scatterers as a factor limiting carrier mobility in graphene, Nano Lett. 10 (2010) 3868–3872.

[22] V. Geringer, M. Liebmann, T. Echtermeyer, S. Runte, M. Schmidt, R. Rückamp, M.C. Lemme, M. Morgenstern, Intrinsic and extrinsic corrugation of monolayer graphene deposited on SiO_{2}, Phys. Rev. Lett. 102 (2009) 076102.

[23] A. Locatelli, K.R. Knox, D. Cvetko, T.O. Menteş, M.A. Niño, S. Wang, M.B. Yilmaz, P. Kim, R.M. Osgood, A. Morgante, Corrugation in exfoliated graphene: an electron microscopy and diffraction study, ACS Nano 4 (2010) 4879–4889.

[24] W. Bao, F. Miao, Z. Chen, H. Zhang, W. Jang, C. Dames, C.N. Lau, Controlled ripple texturing of suspended graphene and ultrathin graphite membranes, Nat Nano 4 (2009) 562–566.

[25] M. Ishigami, J.H. Chen, W.G. Cullen, M.S. Fuhrer, E.D. Williams, Atomic structure of graphene on SiO_2, Nano Lett. 7 (2007) 1643–1648.

[26] J. Martin, N. Akerman, G. Ulbricht, T. Lohmann, J.H. Smet, K. von Klitzing, A. Yacoby, Observation of electron-hole puddles in graphene using a scanning single-electron transistor, Nat. Phys. 4 (2008) 144–148.

[27] V.V. Cheianov, V.I. Fal'ko, Selective transmission of Dirac electrons and ballistic magnetoresistance of n-p junctions in graphene, Phys. Rev. B 74 (2006) 041403.

[28] M.I. Katsnelson, K.S. Novoselov, A.K. Geim, Chiral tunnelling and the Klein paradox in graphene, Nat. Phys. 2 (2006) 620–625.

[29] K.I. Bolotin, F. Ghahari, M.D. Shulman, H.L. Stormer, P. Kim, Observation of the fractional quantum Hall effect in graphene, Nature 462 (2009) 196–199.

[30] X. Du, I. Skachko, F. Duerr, A. Luican, E.Y. Andrei, Fractional quantum Hall effect and insulating phase of Dirac electrons in graphene, Nature 462 (2009) 192–195.

[31] J.G. Checkelsky, L. Li, N.P. Ong, Zero-energy state in graphene in a high magnetic field, Phys. Rev. Lett. 100 (2008) 206801.

[32] M.O. Goerbig, R. Moessner, B. Doucot, Electron interactions in graphene in a strong magnetic field, Phys. Rev. B 74 (2006) 161407.

[33] V.P. Gusynin, V.A. Miransky, S.G. Sharapov, I.A. Shovkovy, Edge states, mass and spin gaps, and quantum Hall effect in graphene, Phys. Rev. B 77 (2008) 205409.

[34] J. Jung, A.H. MacDonald, Theory of the magnetic-field-induced insulator in neutral graphene sheets, Phys. Rev. B 80 (2009) 235417.

[35] K. Yang, Spontaneous symmetry breaking and quantum Hall effect in graphene, Solid State Commun. 143 (2007) 27–32.

[36] Y. Zhang, Z. Jiang, J.P. Small, M.S. Purewal, Y.W. Tan, M. Fazlollahi, J.D. Chudow, J.A. Jaszczak, H.L. Stormer, P. Kim, Landau-level splitting in graphene in high magnetic fields, Phys. Rev. Lett. 96 (2006) 136806.

[37] C.R. Dean, A.F. Young, P. Cadden-Zimansky, L. Wang, H. Ren, K. Watanabe, T. Taniguchi, P. Kim, J. Hone, K.L. Shepard, Multicomponent fractional quantum Hall effect in graphene, Nat. Phys. 7 (2011) 693–696.

[38] Z. Papic, M.O. Goerbig, N. Regnault, Theoretical expectations for a fractional quantum Hall effect in graphene, Solid State Commun. 149 (2009) 1056–1060.

[39] C. Tőke, J.K. Jain, SU(4) composite fermions in graphene: fractional quantum Hall states without analog in GaAs, Phys. Rev. B 75 (2007) 245440.

[40] A.K. Geim, K.S. Novoselov, The rise of graphene, Nat. Mater. 6 (2007) 183–191.

[41] G.W. Semenoff, Condensed-matter simulation of a three-dimensional anomaly, Phys. Rev. Lett. 53 (1984) 2449–2452.

[42] F. Miao, S. Wijeratne, Y. Zhang, U.C. Coskun, W. Bao, C.N. Lau, Phase-coherent transport in graphene quantum billiards, Science 317 (2007) 1530–1533.

[43] J.H. Seol, I. Jo, A.L. Moore, L. Lindsay, Z.H. Aitken, M.T. Pettes, X. Li, Z. Yao, R. Huang, D. Broido, N. Mingo, R.S. Ruoff, L. Shi, Two-dimensional phonon transport in supported graphene, Science 328 (2010) 213–216.

[44] F. Guinea, T. Low, Band structure and gaps of triangular graphene superlattices, Philos. Trans. R. Soc. A Math. Phys. Eng. Sci. 368 (2010) 5391–5402.

[45] J.A. Furst, J.G. Pedersen, C. Flindt, N.A. Mortensen, M. Brandbyge, T.G. Pedersen, A.P. Jauho, Electronic properties of graphene antidot lattices, New J. Phys. 11 (2009).

[46] W. Liu, Z.F. Wang, Q.W. Shi, J. Yang, F. Liu, Band-gap scaling of graphene nanohole superlattices, Phys. Rev. B 80 (2009) 233405.

[47] T.G. Pedersen, C. Flindt, J. Pedersen, N.A. Mortensen, A.P. Jauho, K. Pedersen, Graphene antidot lattices: designed defects and spin qubits, Phys. Rev. Lett. 100 (2008).

[48] R.P. Tiwari, D. Stroud, Tunable band gap in graphene with a noncentrosymmetric superlattice potential, Phys. Rev. B 79 (2009) 205435.

[49] R. Balog, B. Jorgensen, L. Nilsson, M. Andersen, E. Rienks, M. Bianchi, M. Fanetti, E. Laegsgaard, A. Baraldi, S. Lizzit, Z. Sljivancanin, F. Besenbacher, B. Hammer, T.G. Pedersen, P. Hofmann, L. Hornekaer, Bandgap opening in graphene induced by patterned hydrogen adsorption, Nat. Mater. 9 (2010) 315–319.

[50] G. Giovannetti, P.A. Khomyakov, G. Brocks, P.J. Kelly, J. van den Brink, Substrate-induced band gap in graphene on hexagonal boron nitride: ab initio density functional calculations, Phys. Rev. B 76 (2007) 073103.

[51] R. Martinazzo, S. Casolo, G.F. Tantardini, Symmetry-induced band-gap opening in graphene superlattices, Phys. Rev. B 81 (2010) 245420.

[52] J.C. Meyer, C.O. Girit, M.F. Crommie, A. Zettl, Hydrocarbon lithography on graphene membranes, Appl. Phys. Lett. 92 (2008).

[53] J. Bai, X. Zhong, S. Jiang, Y. Huang, X. Duan, Graphene nanomesh, Nat. Nanotechnol. 5 (2010) 190–194.

[54] X. Liang, Y.-S. Jung, S. Wu, A. Ismach, D.L. Olynick, S. Cabrini, J. Bokor, Formation of bandgap and subbands in graphene nanomeshes with sub-10 nm ribbon width fabricated via nanoimprint lithography, Nano Lett. 10 (2010) 2454–2460.

[55] Y. Yang, X. Yang, X. Zho, S. Wu, D. Wan, A. Cao, L. Liao, Q. Yuan, X. Duan, Ultrafine graphene nanomesh with large on/off ratio for high-performance flexible biosensors, Adv. Funct. Mater. 27 (2016) 160496.

[56] Z. Zeng, X. Huang, Z. Yin, H. Li, Y. Chen, H. Li, Q. Zhang, J. Ma, F. Boey, H. Zhang, Fabrication of graphene nanomesh by using an anodic aluminum oxide membrane as a template, Adv. Mater. 24 (2012) 4138–4142.

[57] S.-Y. Son, M. Park, D.S. Lee, S. Lee, J. Han, G.Y. Jung, H.-I. Joh, Field effect in amorphous carbon nanomesh directly synthesized from phase-separated polymer blends, Carbon 142 (2019) 285–290.

[58] T. Feng, X. Ruan, Ultra-low thermal conductivity in graphene nanomesh, Carbon 101 (2016) 107–113.

[59] J. Oh, H. Yoo, J. Choi, J.Y. Kim, D.S. Lee, M.J. Kim, J.-C. Lee, W.N. Kim, J.C. Grossman, J.H. Park, S.-S. Lee, H. Kim, J.G. Son, Significantly reduced thermal conductivity and enhanced thermoelectric properties of single- and bi-layer graphene nanomeshes with sub-10 nm neck-width, Nano Energy 35 (2017) 26–35.

[60] E.V. Castro, K.S. Novoselov, S.V. Morozov, N.M.R. Peres, J.M.B.L. dos Santos, J. Nilsson, F. Guinea, A.K. Geim, A.H.C. Neto, Biased bilayer graphene: semiconductor with a gap tunable by the electric field effect, Phys. Rev. Lett. 99 (2007) 216802.

[61] E. McCann, Asymmetry gap in the electronic band structure of bilayer graphene, Phys. Rev. B 74 (2006) 161403.

[62] H. Min, B. Sahu, S.K. Banerjee, A.H. MacDonald, Ab initio theory of gate induced gaps in graphene bilayers, Phys. Rev. B 75 (2007) 155115.

[63] T. Ohta, A. Bostwick, T. Seyller, K. Horn, E. Rotenberg, Controlling the electronic structure of bilayer graphene, Science 313 (2006) 951–954.

[64] J.B. Oostinga, H.B. Heersche, X.L. Liu, A.F. Morpurgo, L.M.K. Vandersypen, Gate-induced insulating state in bilayer graphene devices, Nat. Mater. 7 (2008) 151–157.

[65] T. Taychatanapat, P. Jarillo-Herrero, Electronic transport in dual-gated bilayer graphene at large displacement fields, Phys. Rev. Lett. 105 (2010).

[66] F. Xia, D.B. Farmer, Y.-M. Lin, P. Avouris, Graphene field-effect transistors with high on/off current ratio and large transport band gap at room temperature, Nano Lett. 10 (2010) 715–718.

[67] Y. Zhang, T.-T. Tang, C. Girit, Z. Hao, M.C. Martin, A. Zettl, M.F. Crommie, Y.R. Shen, F. Wang, Direct observation of a widely tunable bandgap in bilayer graphene, Nature 459 (2009) 820–823.

[68] J. Park, S.B. Jo, Y.-J. Yu, Y. Kim, J.W. Yang, W.H. Lee, H.H. Kim, B.H. Hong, P. Kim, K. Cho, K.S. Kim, Single-gate bandgap opening of bilayer graphene by dual molecular doping, Adv. Mater. 24 (2012) 407–411.

[69] J. Kedzierski, P.L. Hsu, P. Healey, P.W. Wyatt, C.L. Keast, M. Sprinkle, C. Berger, W.A. de Heer, Epitaxial graphene transistors on SIC substrates, IEEE Trans. Electron Devices 55 (2008) 2078–2085.

[70] J. Kedzierski, P.L. Hsu, A. Reina, J. Kong, P. Healey, P. Wyatt, C. Keast, Graphene-on-insulator transistors made using C on Ni chemical-vapor deposition, IEEE Electron Device Lett. 30 (2009) 745–747.

[71] M.C. Lemme, T.J. Echtermeyer, M. Baus, H. Kurz, A graphene field-effect device, IEEE Electron Device Lett. 28 (2007) 282–284.

[72] X. Li, W. Cai, J. An, S. Kim, J. Nah, D. Yang, R. Piner, A. Velamakanni, I. Jung, E. Tutuc, S.K. Banerjee, L. Colombo, R.S. Ruoff, Large-area synthesis of high-quality and uniform graphene films on copper foils, Science 324 (2009) 1312–1314.

[73] L. Liao, J.W. Bai, Y.Q. Qu, Y.C. Lin, Y.J. Li, Y. Huang, X.F. Duan, High-kappa oxide nanoribbons as gate dielectrics for high mobility top-gated graphene transistors, Proc. Natl. Acad. Sci. U. S. A. 107 (2010) 6711–6715.

[74] Y.-M. Lin, C. Dimitrakopoulos, K.A. Jenkins, D.B. Farmer, H.-Y. Chiu, A. Grill, P. Avouris, 100-GHz transistors from wafer-scale epitaxial graphene, Science 327 (2010) 662.

[75] Y.-M. Lin, K.A. Jenkins, A. Valdes-Garcia, J.P. Small, D.B. Farmer, P. Avouris, Operation of graphene transistors at gigahertz frequencies, Nano Lett. 9 (2008) 422–426.

[76] I. Meric, M.Y. Han, A.F. Young, B. Ozyilmaz, P. Kim, K.L. Shepard, Current saturation in zero-bandgap, top-gated graphene field-effect transistors, Nat. Nanotechnol. 3 (2008) 654–659.

[77] J.S. Moon, D. Curtis, M. Hu, D. Wong, C. McGuire, P.M. Campbell, G. Jernigan, J.L. Tedesco, B. Vanmil, R. Myers-Ward, C. Eddy, D.K. Gaskill, Epitaxial-graphene RF field-effect transistors on Si-face 6H-SiC substrates, IEEE Electron Device Lett. 30 (2009) 650–652.

[78] H. Yang, J. Heo, S. Park, H.J. Song, D.H. Seo, K.-E. Byun, P. Kim, I. Yoo, H.-J. Chung, K. Kim, Graphene barristor, a triode device with a gate-controlled Schottky barrier, Science 336 (2012) 1140–1143.

[79] M. Ezawa, Peculiar width dependence of the electronic properties of carbon nanoribbons, Phys. Rev. B 73 (2006) 045432.

[80] M. Fujita, K. Wakabayashi, K. Nakada, K. Kusakabe, Peculiar localized state at zigzag graphite edge, J. Phys. Soc. Jpn. 65 (1996) 1920–1923.

[81] K. Nakada, M. Fujita, G. Dresselhaus, M.S. Dresselhaus, Edge state in graphene ribbons: nanometer size effect and edge shape dependence, Phys. Rev. B 54 (1996) 17954–17961.

[82] K. Wakabayashi, M. Fujita, H. Ajiki, M. Sigrist, Electronic and magnetic properties of nanographite ribbons, Phys. Rev. B 59 (1999) 8271–8282.

[83] Y.-W. Son, M.L. Cohen, S.G. Louie, Energy gaps in graphene nanoribbons, Phys. Rev. Lett. 97 (2006) 216803.

[84] B. Krauss, P.T. Nemes-Incze, V. Skakalova, L.S.P. Biro, K. von Klitzing, J.H. Smet, Raman scattering at pure graphene zigzag edges, Nano Lett. 10 (2010) 4544–4548.

[85] Z.H. Chen, Y.M. Lin, M.J. Rooks, P. Avouris, Graphene nano-ribbon electronics, Physica E Low Dimens. Syst. Nanostruct. 40 (2007) 228–232.

[86] M.Y. Han, B. Özyilmaz, Y. Zhang, P. Kim, Energy band-gap engineering of graphene nanoribbons, Phys. Rev. Lett. 98 (2007) 206805.

[87] K. Todd, H.-T. Chou, S. Amasha, D. Goldhaber-Gordon, Quantum dot behavior in graphene nanoconstrictions, Nano Lett. 9 (2008) 416–421.

[88] P. Darancet, V. Olevano, D. Mayou, Coherent electronic transport through graphene constrictions: subwavelength regime and optical analogy, Phys. Rev. Lett. 102 (2009) 136803.

[89] F. Muñoz-Rojas, D. Jacob, J. Fernández-Rossier, J.J. Palacios, Coherent transport in graphene nanoconstrictions, Phys. Rev. B 74 (2006) 195417.

[90] F. Molitor, A. Jacobsen, C. Stampfer, J. Güttinger, T. Ihn, K. Ensslin, Transport gap in side-gated graphene constrictions, Phys. Rev. B 79 (2009) 075426.

[91] B. Terres, J. Dauber, C. Volk, S. Trellenkamp, U. Wichmann, C. Stampfer, Disorder induced Coulomb gaps in graphene constrictions with different aspect ratios, Appl. Phys. Lett. (2011) 98.

[92] N. Tombros, A. Veligura, J. Junesch, M.H.D. Guimaraes, I.J. Vera-Marun, H.T. Jonkman, B.J. van Wees, Quantized conductance of a suspended graphene nanoconstriction, Nat. Phys. 7 (2011) 697–700.

[93] N.S. Safron, A.S. Brewer, M.S. Arnold, Semiconducting two-dimensional graphene nanoconstriction arrays, Small 7 (2011) 492–498.

[94] L. Brey, H.A. Fertig, Electronic states of graphene nanoribbons studied with the Dirac equation, Phys. Rev. B 73 (2006) 235411.

[95] P. Nemes-Incze, G. Magda, K. Kamaras, L.P. Biro, Crystallographically selective nanopatterning of graphene on SiO$_2$, Nano Res. 3 (2010) 110–116.

[96] L. Xie, L. Jiao, H. Dai, Selective etching of graphene edges by hydrogen plasma, J. Am. Chem. Soc. 132 (2010) 14751–14753.

[97] X. Wang, H. Dai, Etching and narrowing of graphene from the edges, Nat. Chem. 2 (2010) 661–665.

[98] L. Liu, Y.L. Zhang, W.L. Wang, C.Z. Gu, X.D. Bai, E.G. Wang, Nanosphere lithography for the fabrication of ultranarrow graphene nanoribbons and on-chip bandgap tuning of graphene, Adv. Mater. 23 (2011) 1246.

[99] Y. Lu, B. Goldsmith, D.R. Strachan, J.H. Lim, Z.T. Luo, A.T.C. Johnson, High-on/off-ratio graphene nanoconstriction field-effect transistor, Small 6 (2010) 2748–2754.

[100] R. Yang, L.C. Zhang, Y. Wang, Z.W. Shi, D.X. Shi, H.J. Gao, E.G. Wang, G.Y. Zhang, An anisotropic etching effect in the graphene basal plane, Adv. Mater. 22 (2010) 4014–4019.

[101] L.A. Ponomarenko, F. Schedin, M.I. Katsnelson, R. Yang, E.W. Hill, K.S. Novoselov, A.K. Geim, Chaotic Dirac billiard in graphene quantum dots, Science 320 (2008) 356–358.

[102] J.H. Bardarson, M. Titov, P.W. Brouwer, Electrostatic confinement of electrons in an integrable graphene quantum dot, Phys. Rev. Lett. 102 (2009) 226803.

[103] S. Schnez, F. Molitor, C. Stampfer, J. Guttinger, I. Shorubalko, T. Ihn, K. Ensslin, Observation of excited states in a graphene quantum dot, Appl. Phys. Lett. 94 (2009).

[104] S. Droscher, H. Knowles, Y. Meir, K. Ensslin, T. Ihn, Coulomb gap in graphene nanoribbons, Phys. Rev. B 84 (2011).

[105] J. Guettinger, C. Stampfer, S. Hellmueller, F. Molitor, T. Ihn, K. Ensslin, Charge detection in graphene quantum dots, Appl. Phys. Lett. 93 (2008).

[106] C. Stampfer, E. Schurtenberger, F. Molitor, J. Guettinger, T. Ihn, K. Ensslin, Tunable graphene single electron transistor, Nano Lett. 8 (2008) 2378–2383.

[107] S. Jung, G.M. Rutter, N.N. Klimov, D.B. Newell, I. Calizo, A.R. Hight-Walker, N.B. Zhitenev, J.A. Stroscio, Evolution of microscopic localization in graphene in a magnetic field from scattering resonances to quantum dots, Nat. Phys. 7 (2011) 245–251.

[108] X.L. Liu, D. Hug, L.M.K. Vandersypen, Gate-defined graphene double quantum dot and excited state spectroscopy, Nano Lett. 10 (2010) 1623–1627.

[109] F. Molitor, H. Knowles, S. Droescher, U. Gasser, T. Choi, P. Roulleau, J. Guettinger, A. Jacobsen, C. Stampfer, K. Ensslin, T. Ihn, Observation of excited states in a graphene double quantum dot, EPL 89 (2010).

[110] G. Luo, Z.-Z. Zhang, G.-W. Deng, H.-O. Li, G. Cao, M. Xiao, G.-C. Guo, G.-P. Guo, Coupling graphene nanomechanical motion to a single-electron transistor, Nanoscale 9 (2017) 5608–5614.

[111] J. Velasco Jr., J. Lee, D. Wong, S. Kahn, H.-Z. Tsai, J. Costello, T. Umeda, T. Taniguchi, K. Watanabe, A. Zettl, F. Wang, M.F. Crommie, Visualization and control of single electron charging in bilayer graphene quantum dots, Nano Lett. 18 (2018) 5104–5110.

[112] B. Trauzettel, D.V. Bulaev, D. Loss, G. Burkard, Spin qubits in graphene quantum dots, Nat. Phys. 3 (2007) 192–196.

[113] J. Martin, N. Akerman, G. Ulbricht, T. Lohmann, K. von Klitzing, J.H. Smet, A. Yacoby, The nature of localization in graphene under quantum Hall conditions, Nat. Phys. 5 (2009) 669–674.

[114]

D.S. Lee, V. Skakalova, R.T. Weitz, J.H. Smet, K. von Klitzing, Transconductance fluctuations as a probe for interaction-induced quantum Hall states in graphene, Phys. Rev. Lett. 109 (2012) 056602.

[115] D.H. Cobden, C.H.W. Barnes, C.J.B. Ford, Fluctuations and evidence for charging in the quantum Hall effect, Phys. Rev. Lett. 82 (1999) 4695–4698.

[116] S. Branchaud, A. Kam, P. Zawadzki, F.M. Peeters, A.S. Sachrajda, Transport detection of quantum Hall fluctuations in graphene, Phys. Rev. B 81 (2010) 121406.

[117] J. Velasco Jr., G. Liu, L. Jing, P. Kratz, H. Zhang, W. Bao, M. Bockrath, C.N. Lau, Probing charging and localization in the quantum Hall regime by graphene p–n–p junctions, Phys. Rev. B 81 (2010) 121407.

[118] E.R. Mucciolo, C.H. Lewenkopf, Disorder and electronic transport in graphene, J. Phys. Condens. Matter 22 (2010).

Abstract

The chapter describes single charge tunneling behavior in graphene devices. Coulomb blockade phenomena observed in graphene constrictions, patterned single electron transistors, and graphene nanoribbons are compared with those observed in the conventional single electron transistors with metallic islands. This chapter also covers the phenomena when compressible quantum dots are formed in graphene in the quantum Hall regime such as mesoscopic conductance fluctuations due to single charge tunneling into/out of the quantum dots.

Queries and Answers

Q1

Query: Per guidelines, figure part labels (a), (b), (c) should be in upper case (i.e., (A), (B), (C)). Hence please check and update the figure part labels and also the indicators provided for sublattices in the caption of Fig. 5.4.

Answer: I can do the caption only. The figure hase to be send to the author: Dong Su Lee (not me - the editor)

Q2

Query: Please check the caption and artwork of Fig. 5.12 for correctness.

Answer: done

Q3

Query: Panel labels "(A)–(C)" are mentioned in the Fig. 5.19 caption but are not found in the figure artwork. Please check.

Answer: *Fig. 5.19 Greyscale rendition* of transconductance g_m in the (n, B)-plane. (Printed from [114])

Q4

Query: Please check that we have captured author name and affiliation details correctly.

Answer: ok

Q5

Query: Please check all the section number citations present in the text for correctness.

Answer: seem ok

Q6

Query: Please check if the insertion of Fig. 5.3 citation is OK, or suggest an alternative location if necessary.

Answer: (Fig. 5.3) should be removed from the current location and placed after "....so-called Coulomb diamonds..."

Q7

Query: Please check the Eq. (5.4) for correctness.

Answer: Correct

Q8

Query: Equations have been renumbered as Eq. (5.4) occurred more than once. Please check, and correct if necessary.

Answer: Correct

Q9

Query: In the sentence "In transport measurements, graphene linear dispersion relation therefore holds." please confirm edits are correct.

Answer: correct

Q10

Query: In the sentence that begins "The lower two insets of Fig. 5.6 show optical images of the device ..." please confirm edits are correct.

Answer: The sentence should be: "....and the device grown on a metal substrate ....", without "is".

Q11

Query: The citation "Fig. 6(d)" has been changed to "Fig. 5.6". Please check if this change is appropriate, and amend if necessary.

Answer: correct

Q12

Query: Per Elsevier guideline, Prefix words should not be hyphenated (e.g., anti, non, quasi, sub, etc.) and the same has been followed in this chapter. Please check.

Answer: ok

Q13

Query: In the sentence that begins "Depending on the boundary conditions, if some of the one-dimensional modes cross ..." please check the wording. Uncertain of how to change the sentence to reflect intended meaning.

Answer: I would change the sentence as follows: Depending on the boundary conditions, if some of the one-dimensional modes cross the Dirac point, then the ribbon shows metallic behavior, although otherwise it is semiconducting with a finite energy gap.

Q14

Query: Please check if the insertion of Fig. 5.12 citation is OK, or suggest an alternative location if necessary.

Answer: It is corrected in the text

Q15

Query: Please check if the insertion of Fig. 5.14 citation is OK, or suggest an alternative location if necessary.

Answer: correct

Q16

Query: Please check if the insertion of Fig. 5.16 citation is OK, or suggest an alternative location if necessary.

Answer: (Fig. 5.16) moved in the text

Q17

Query: The term "qbits" has been changed to "qubits". Please check if this change is appropriate, and amend if necessary.

Answer: ok

Q18

Query: In the sentence that ends with "... while such states are invisible or only seen as faint signatures if visible." Please clarify the wording at the end of the sentence. Uncertain of how to change to reflect intended meaning.

Answer: corrected (suggested) in the text

Q19

Query: The citation "Fig. 3f" has been changed to "Fig. 5.23". Please check if this change is appropriate, and amend if necessary.

Answer: correct

Q20

Query: Please check the inserted book title for reference [4], and correct if necessary.

Answer: corrected

Q21

Query: Please check the inserted journal title for reference [57], and correct if necessary.

Answer: The journal is Carbon